Low-Loss Monolithic Transmission Lines for Submillimeter and Terahertz Frequency Applications

Andrew G. Engel, Jr. and Linda P. B. Katehi, *Senior Member, IEEE*

Abstract—**The design and construction of low-loss monolithic transmission lines are critical to systems which require that THz-power be guided to the antenna front-ends. This paper proposes two types of novel monolithic guiding structures, which are designed for the 0.3–2.0 THz and 0.1–0.3 THz ranges, respectively. The new waveguides are constructed from dielectric materials and structures which are available in monolithic technology so that the integration of active devices is possible. Propagation in each of the waveguides is characterized over relevant frequency ranges by applying a mode-matching technique, which takes into account all forms of electromagnetic coupling as well as losses in the dielectrics. The structures are predicted to exhibit excellent power confinement and low losses.**

I. Introduction

TECHNOLOGY based on the frequency range of 0.1–2.0 THz offers narrow-beam, high-resolution antennas which are essential for intelligent computer control guidance, command systems for space applications, and sensors which operate in optically opaque media. Since these systems require that the generated THz-power be guided to the antenna front-end through complex feeding networks, the design and construction of low-loss monolithic transmission lines are critical.

There are two typical approaches for the design of these transmission lines. The first approach extends the use of planar conductors in monolithic millimeter wave technology to higher frequencies. Planar circuit elements such as loads, transitions, junctions and lines perform quite well at frequencies up to 100 GHz, but ohmic and radiation losses become unacceptably high as the frequency increases further. The second approach extends optical techniques to lower frequencies. This approach is hindered by three factors. First, optical materials are usually incompatible with the semiconducting materials which are needed for active devices. Second, phenomena which dominate optical waves, such as nonlinear wave characteristics, are not present at terahertz frequencies. Finally, phenomena which are ignored at optical frequencies, such as radiation and electromagnetic coupling, are not negligible at terahertz frequencies.

A different approach is established by examining the millimeter wave dielectric waveguides which were extensively investigated in the 1970's and early 1980's. Examples of these waveguides include dielectric image guides [3], strip dielectric guides, insulated image guides, strip-slab guides [4], inverted strip dielectric guides [6], cladded image guides [5], and trapped image guides [7]. The waveguides are constructed from combinations of layers and ridges of various permittivities in order to provide a region wherein the propagating power is well-confined. The widths of the lines approach one guided wavelength in order to maximize field confinement. Although there are several examples of the monolithic use of dielectric waveguides in the literature (e.g., [8]), these waveguides have been generally considered hybrid in nature.

Monolithic sub-mm and THz guiding structures may be realized by considering variations of the early dielectric waveguides. The new waveguides are constructed from dielectric materials and structures which are available in monolithic technology so that the use of the waveguides in integrated circuits is possible. The dimensions of the waveguides are on the order of a fraction of a guided wavelength, so that the new structures may be used not only as transmission lines, but also as passive circuit elements such as inductors and couplers. Since the proposed structures will have properties similar to conventional microstrip elements, the structures will be able to provide both low-loss feeding networks and highly efficient radiating elements for arrays.

In the succeeding sections, two types of monolithic guiding structures are described. The two types are designed for specific frequencies in the 0.3–2.0 THz and 0.1–0.3 THz ranges, respectively. Propagation in each of the waveguides is characterized over relevant frequency ranges by applying a mode-matching technique, which takes into account all forms of electromagnetic coupling as well as losses in the dielectrics.

Manuscript received February 7, 1991; revised July 9, 1991. This work was supported by the Army Research Office under the URI program, Contract no. DAAL-3087-K-0007, and by the NASA Center for Space Terahertz Technology.

The authors are with the Radiation Laboratory, Electrical Engineering and Computer Science Department, The University of Michigan, 1301 Beal Ave., Ann Arbor, MI 48109-2122.

IEEE Log Number 9103096.

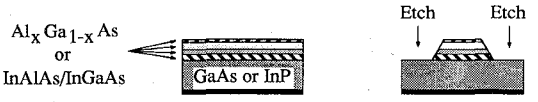

Fig. 1. Ridged example of 0.3–2.0 THz waveguide.

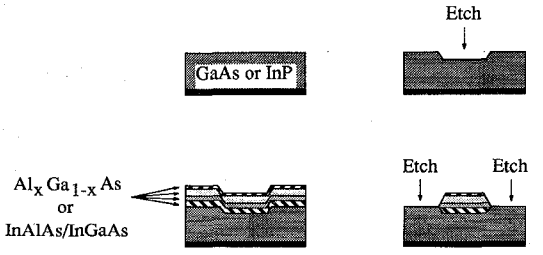

Fig. 2. Semi-embedded example of 0.3–2.0 THz waveguide.

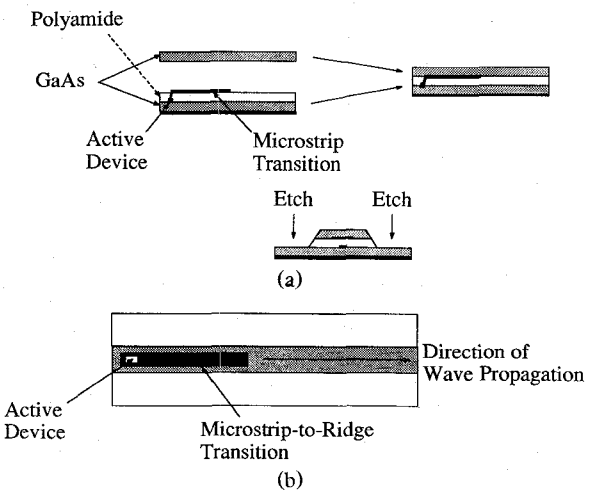

Fig. 3. Example of 0.1–0.3 THz waveguide, including the integration of an active device and its transition. (a) Side view. (b) Top view.

II. Proposed Construction

The proposed structures, shown in Figs. 1–3, consist of alternating layers of high and low permittivities. The abrupt changes in the permittivities in the x-direction are designed to optimize power confinement in the layer with the lowest permittivity. This layer, designated the *propagation layer*, is away from the ground plane, resulting in minimal ground plane conductor loss. A ridge or a semi-embedded strip provides power confinement in the y-direction.

The structures in Figs. 1 and 2 are suitable for the 0.3–2.0 THz region. The structures may be either ridged or semi-embedded and will be made of semiconducting materials grown on GaAs or InP substrates. The ridged structure is created by etching a layered wafer. The semi-embedded waveguide is fabricated by etching a well of appropriate dimensions into a semiconducting substrate, filling the well with layers of intrinsic semiconducting materials using regrowth techniques, and etching again. In both the ridged and the semi-embedded structures, layers of 5–10 μ are required, and these layers can be provided by MOCVD.

As the frequency of operation decreases, thicker layers are required and the times required to grow the layers on the wafers become impractically large. Hence, a second type of waveguide is proposed for the sub-mm wave region (0.1–0.3 THz). This structure is constructed from a combination of semiconducting substrates and dielectric films. In the example shown in Fig. 3, a wafer of GaAs is covered with a polyamide film, attached to another GaAs wafer with a thin epoxy glue, and etched to produce a ridged waveguide. The epoxy is expected to create a gap of approximately 1 μ, which would not affect the propagation characteristics. A similar structure could be created with silicon wafers and a quartz film; in this case, the wafers are attached with electrobonding.

Given the aforementioned construction of the proposed waveguides, the fabrication of integrated circuits which use the waveguides as interconnects is conceivable. For example, an active device may be integrated with the 0.1–0.3 THz waveguide by manufacturing the device in the position shown in Fig. 3. This step is performed prior to the addition of the polyamide layer; the subsequent construction of the layers and the etching to create the ridged structure may be done without damaging the active device. An active device may be integrated with a 0.3–2.0 THz waveguide in a similar fashion, but the addition of high quality, low-loss layers after the device has been manufactured may be troublesome if the process used to add the layers requires temperatures which are high enough to damage the active device. Several alternatives exist for the design of a transition between an active device and a waveguide. The similarity between the dominant mode of the dielectric waveguide and the dominant mode in microstrip and the ease with which a transition between microstrip and an active device may be accomplished suggests that a transition could consist of a short length of microstrip near a device (Fig. 3). Another design could employ a vertical probe extending upward from the device into the propagation layer. A combination of the above alternatives could also be used as a transition. The device could be biased using side feeds which are perpendicular to the direction of propagation. Passive structures such as couplers, stubs, T-junctions, and inductors may be created by fabricating the transmission lines in the desired pattern on the substrate and selectively adding metallization to add inductance or improve power confinement. The various theoretical and experimental issues associated with the use of these waveguides in integrated circuits are suitable topics for future work.

III. Theory

The propagation constants γ and fields of the proposed lines have been analyzed using a mode-matching method, similar to the ones employed in [1]–[3], [9], [10], [11]. The general structure, shown in Fig. 4, is created by assuming the sidewalls of the waveguides are parallel to the x-axis. The nature of the etching process will cause the actual waveguide sidewalls to be angled with respect to the x-axis, but, given the very small height of the propagation

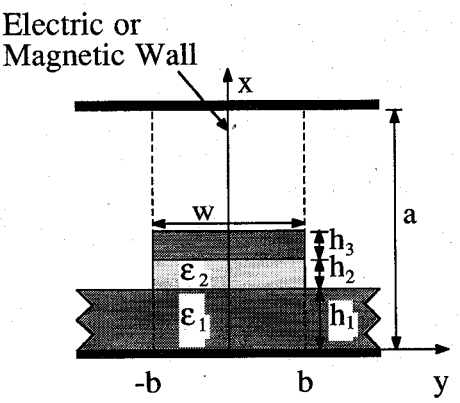

Fig. 4. General structure for mode matching analysis.

layer, this approximation will not significantly alter the results. The structure is uniform in the z-direction. Along the y-axis, the structure is divided into sections at $y = \pm b$. Each section is divided into layers along the x-axis at $x = h_1$, $h_1 + h_2$ and $h_1 + h_2 + h_3$. Each layer is characterized by its permittivity ϵ; losses are accounted for with a complex permittivity $\epsilon = \epsilon_o \epsilon'(1.0 - j \tan \delta)$. The outer sections ($|y| > b$) extend to $y = \pm\infty$. The structure employs perfectly-conducting plates as top and bottom boundaries. The lower plate serves as a ground plane. The upper plate exists so that the mode-matching analysis may be easily applied, but it is placed far enough away from the guiding structure so as to not affect the guidance properties. Using symmetry, the structure can be simplified by adding either a magnetic or electric wall in the middle and only considering half of the structure. For this formulation, the ranges $y < -b$ and $-b < y < 0$ are designated as sections 1 and 2, respectively.

Each section of the structure is a section of an inhomogeneous parallel plate waveguide, which supports TE_x and TM_x modes. The vector potentials $\bar{A} = a_x \hat{x}$ and $\bar{F} = f_x \hat{x}$ generate the fields via

$$\bar{E} = -j\omega\bar{A} + \frac{1}{j\omega\epsilon\mu}\nabla\nabla\cdot\bar{A} + \frac{1}{\epsilon}\nabla\times\bar{F} \tag{1}$$

$$\bar{H} = \frac{1}{\mu}\nabla\times\bar{A} + j\omega\bar{F} - \frac{1}{j\omega\epsilon\mu}\nabla\nabla\cdot\bar{F}. \tag{2}$$

Assuming propagation in the z-direction of the form $e^{-\gamma z}$ and solving the wave equation gives the following infinite summations as solutions for the vector potentials:

$$\tilde{a}_x = \sum_l \psi_l^{ijM}(x)\phi_l^{jM}(y)e^{-\gamma z} \tag{3}$$

$$\tilde{f}_x = \sum_l \psi_l^{ijE}(x)\phi_l^{jE}(y)e^{-\gamma z} \tag{4}$$

where i indicates the layer, j indicates the section, and the superscripts E and M refer to TE_x and TM_x modes, respectively. Considering first the TE_x modes, the functions $\psi_l^{ijE}(x)$ and $\phi_l^{jE}(y)$ are given by

$$\psi_l^{ijE}(x) = A_l^{ijE}\cos k_{xl}^{ijE}x + B_l^{ijE}\sin k_{xl}^{ijE}x. \tag{5}$$

$$\phi_l^{jE}(y) = \begin{cases} C_l^{1E}\exp\left(jk_{yl}^{1E}y\right) & \text{section 1} \\ C_l^{2E}\cos k_{yl}^{2E}y + D_l^{2E}\sin k_{yl}^{2E}y & \text{section 2} \end{cases}. \tag{6}$$

The constants C_l^{jE} and D_l^{jE} are sometimes referred to as mode amplitudes. The wavenumbers $k_{xl}^{ijE}, k_{yl}^{jE}$ and the propagation constant γ satisfy the dispersion relation

$$\left(k^{ij}\right)^2 = \omega^2\epsilon^{ij}\mu^{ij} = \left(k_{xl}^{ijE}\right)^2 + \left(k_{yl}^{jE}\right)^2 - (\gamma)^2. \tag{7}$$

The propagation constant γ is constant for all i, j; k_{yl}^{jE}, C_l^{jE}, and D_l^{jE} are constant for all layers i in section j; and k_{xl}^{ijE}, A_l^{ijE}, and B_l^{ijE} depend on both the section and layer indices. In a given section j with any two layers i and i', k_{xl}^{ijE} and $k_{xl}^{i'jE}$ are related by

$$\left(k^{ij}\right)^2 - \left(k_{xl}^{ijE}\right)^2 = \left(k^{i'j}\right)^2 - \left(k_{xl}^{i'jE}\right)^2. \tag{8}$$

Similar relations hold for the TM_x modes.

Boundary conditions at all interfaces are applied to determine the unknown constants A_l^{ijE}, B_l^{ijE}, C_l^{jE}, D_l^{jE}, A_l^{ijM}, B_l^{ijM}, C_l^{jM}, and D_l^{jM}. Each mode can be shown to individually satisfy the boundary conditions at $x = a_i$, so that the x-dependence of each mode in each section is determined to within one constant per mode. (E.g., the constants associated with the x-dependence of the lth TE_x mode in the layers above layer 1 may be determined in terms of A_l^{1jE}.) The boundary conditions at $x = a_i$ also yield transcendental equations for the x-directed wavenumbers k_{xl}^{ijE} and k_{xl}^{ijM} [12]. Mode matching is utilized at $y = -b$, giving a matrix equation which relates the mode amplitudes in section 1 to the mode amplitudes in section 2. A homogeneous system of equations results from the boundary conditions at $y = 0$. Values for the propagation constant are ascertained from zeros of the determinant of the system. The homogeneous system may then be solved for the mode amplitudes.

In general, the propagation constant γ is complex and may be expressed in terms of the phase constant β and the attenuation constant α as

$$\gamma = \alpha + j\beta. \tag{9}$$

When γ is real ($\alpha \neq 0$, $\beta = 0$), the mode is non-propagating. When γ is imaginary ($\alpha = 0$, $\beta \neq 0$), the mode is a propagating mode, all the power is bound to the waveguide, and the power propagates in the z-direction. When γ is complex ($\alpha \neq 0$, $\beta \neq 0$), the mode is also a propagating mode, but the mode leaks, and power propagates at an angle away from the z-axis into the surrounding substrate. If the dominant mode is leaky, deleterious crosstalk effects could be significant.

The frequency range at which leakage occurs is evaluated by considering the waveguide structure as two regions, namely, the waveguide and the surrounding substrate [10], [11]. In the waveguide, a propagating mode is a plane wave traveling at some angle to the z-axis and the effective index of refraction $n_{\text{eff}1}$ of this mode is equiva-

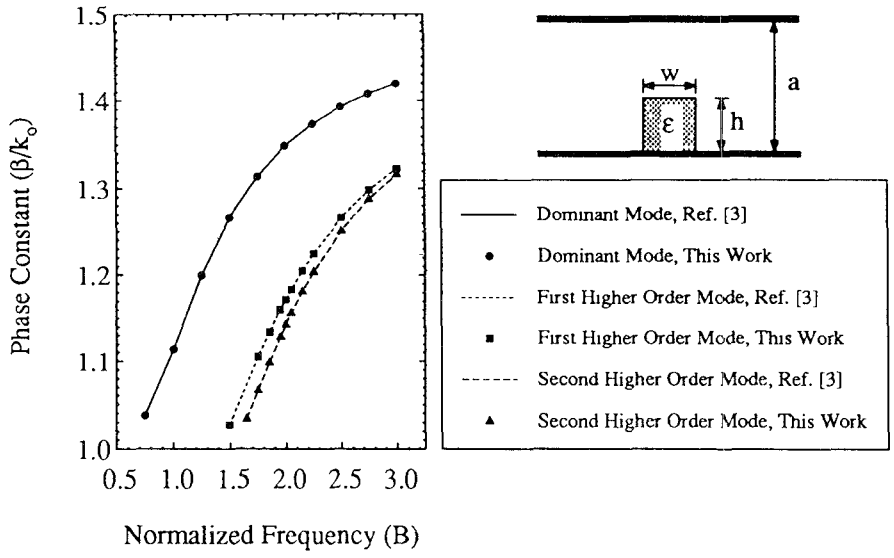

(a)

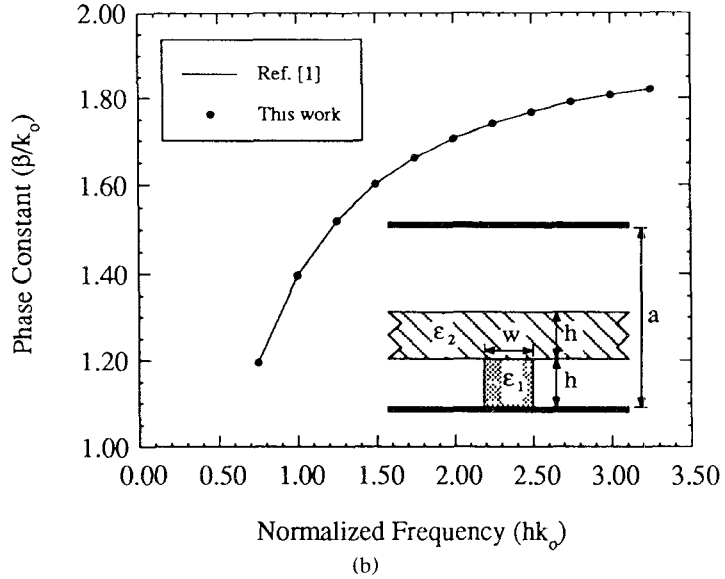

(b)

Fig. 5. Software verification by comparison to previous work. (a) Phase constant β/k_o versus normalized frequency B, compared to reference [3]. $\epsilon = 2.22\epsilon_o$, $h = 4.100$ mm, $w = 4.095$ mm, $a = 19.680$ mm, $B = 2k_o h\sqrt{\epsilon/\epsilon_o - 1}/\pi$, $k_o = \omega\sqrt{\epsilon_o\mu_o}$. (b) Phase constant β/k_o versus normalized frequency hk_o, compared to [1]. $\epsilon_1 = 3.8\epsilon_o$, $\epsilon_2 = 2.1\ \epsilon_o$, $h = 3.33$ mm, $w = 8.40$ mm, $a = 20.00$ mm.

lent to the phase constant β/k_o. In the surrounding dielectric slab, when the dominant TM_{z0} mode is excited, it propagates with effective index of refraction $n_{\text{eff}2}$. For a non-leaky plane wave in the waveguide, $n_{\text{eff}1} > n_{\text{eff}2}$, so each time this wave hits a waveguide side wall (i.e., $y = \pm b$), the wave undergoes total internal reflection. Conversely, for a leaky plane wave, $n_{\text{eff}1} < n_{\text{eff}2}$, so each time this wave hits a side wall, part of the wave reflects and part of the wave is transmitted into the surrounding dielectric substrate. The frequency range at which leakage occurs is determined by calculating $n_{\text{eff}2}$ [14] as a function of frequency and comparing with $n_{\text{eff}1}$.

Roots of the transcendental equations for k_{xl}^{ijE} and k_{xl}^{ijM} and roots of the determinant of the homogeneous system as a function of γ were calculated using various software packages. When small losses in a dielectric region were considered, the root-finding routines were employed using the values obtained from the lossless cases as initial guesses.

Verification of the software was accomplished by comparing with the numerical and experimental results given in [1]–[3]. Examples are given in Fig. 5. Convergence of the propagation constants to within 0.1 percent was easily achieved using 18 TE_y and 18 TM_x modes in each section.

IV. Results

The design parameters and characterization of an example of each type of guiding structure are given in Figs. 6–9. The structures are designed specifically for 94 and

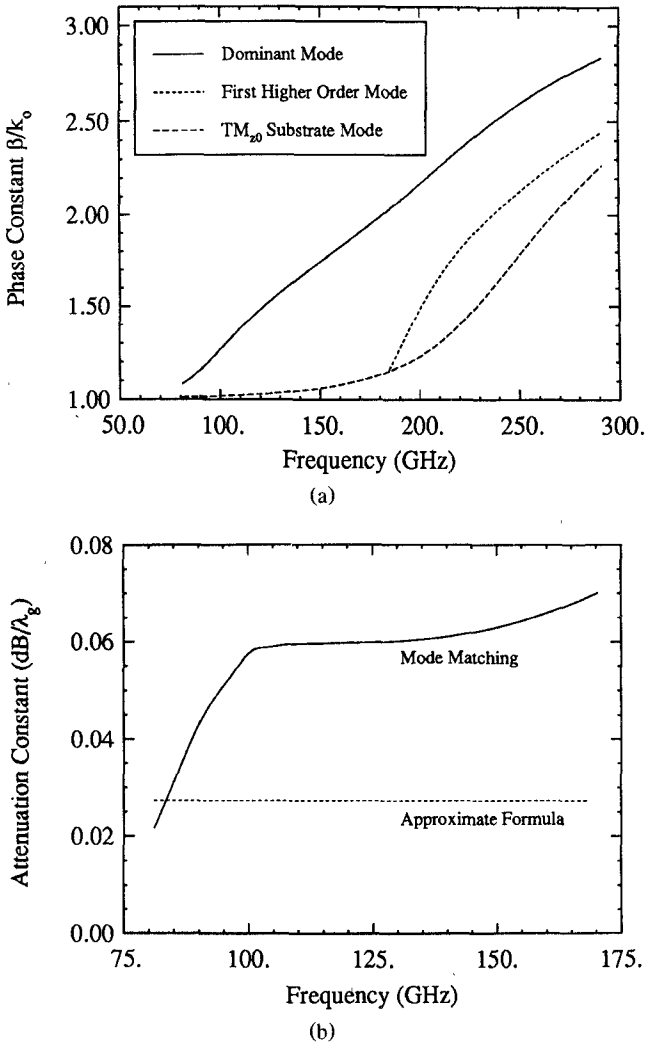

Fig. 6. Propagation constant of the structure designed for 94 GHz. Referring to Fig. 4, $h_1 = 0.032\lambda_g$ (86.4 μm), $h_2 = 0.049\lambda_g$ (130 μm), $h_3 = 0.116\lambda_g$ (309 μm), $w = 0.091\lambda_g$ (241 μm), $a = 0.863\lambda_g$ (2.31 mm), $\epsilon_1 = 12.85\epsilon_o$ (GaAs), $\epsilon_2 = 3.0\epsilon_o$ (polyamide). (a) Phase constant as a function of frequency. (b) Upper bound of attenuation constant as a function of frequency with worst-case dielectric losses ($\epsilon_1 = 12.85\epsilon_o$ $(1.0 - j0.002)$ (GaAs) and $\epsilon_2 = 3.0\ \epsilon_o(1.0 - j0.001)$ (polyamide)).

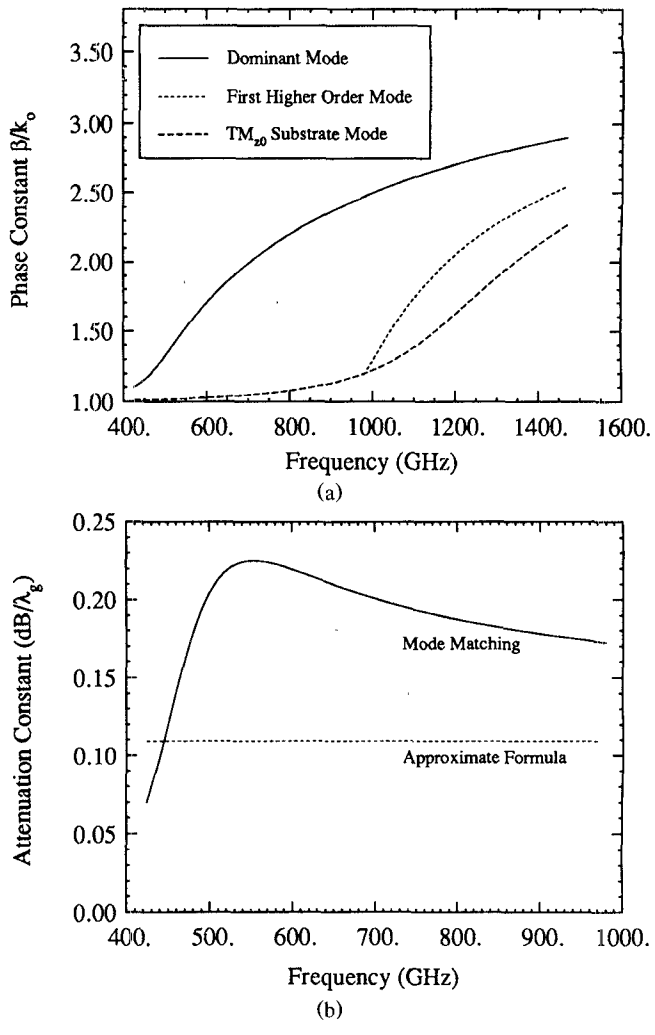

Fig. 7. Propagation constant of the structure designed for 490 GHz. Referring to Fig. 4, $h_1 = 0.036\lambda_g$ (17.1 μm), $h_2 = 0.048\lambda_g$ (22.7 μm), $h_3 = 0.122\lambda_g$ (58.2 μm), $w = 0.064\lambda_g$ (30.6 μm), $a = 0.965\lambda_g$ (459 μm), $\epsilon_1 = 12.85\epsilon_o$ (GaAs), $\epsilon_2 = 10.0\epsilon_o$ (AlAs) [13]. (a) Phase constant as a function of frequency. (b) Upper bound of attenuation constant as a function of frequency with worst-case dielectric losses ($\epsilon_1 = 12.85\epsilon_o$ $(1.0 - j0.004)$ (GaAs) and $\epsilon_2 = 10.0\epsilon_o(1.0 - j0.004)$ (AlAs)).

490 GHz, respectively. Each structure has a GaAs substrate with a ground plane; the 94 GHz waveguide consists of layers of polyamide and GaAs, and the 490 GHz waveguide consists of layers of AlAs and GaAs. Although the substrate of the 490 GHz waveguide is extremely thin (17.1 μm), the substrate/ground plane configuration can be realized by growing a layer of intrinsic GaAs on another highly conductive wafer. The dimensions of the propagation layers at the design frequencies are on the order of 1/10th of a guided wavelength $\lambda_g (= 2\pi/\beta)$.

Plots of the phase constant versus frequency for the dominant and first higher order modes of the 94 GHz structure are shown in Fig. 6(a). The dominant mode has no cut-off frequency, while the first higher order mode cuts off at approximately 180 GHz. Similar results hold for the 490 GHz structure (Fig. 7(a)), where the first higher order mode cuts off at 960 GHz.

Included in Fig. 6(a) is a frequency plot of the phase constant ($\equiv n_{\text{eff}2}$) of the dominant TM_{z0} mode of the surrounding dielectric substrate. As discussed in the previous section, a comparison of $n_{\text{eff}2}$ with the phase constants of the dominant and first order modes of the 94 GHz waveguide determines if and when either of these waveguide modes leaks; clearly, the dominant mode does not leak and the first higher order mode is leaky from its cut-off frequency up to 183 GHz. Similarly, the dominant mode of the 490 GHz waveguide is not leaky and the first higher order mode is leaky from cut-off to 980 GHz (Fig. 7(a)).

Field investigations show that both the dominant and first higher order modes are TM_z-like modes, with dominant electric field components in the x-direction. The dominant mode is very similar to a typical microstrip mode, so that the aforementioned coupling to active devices via short lengths of microstrip is achievable.

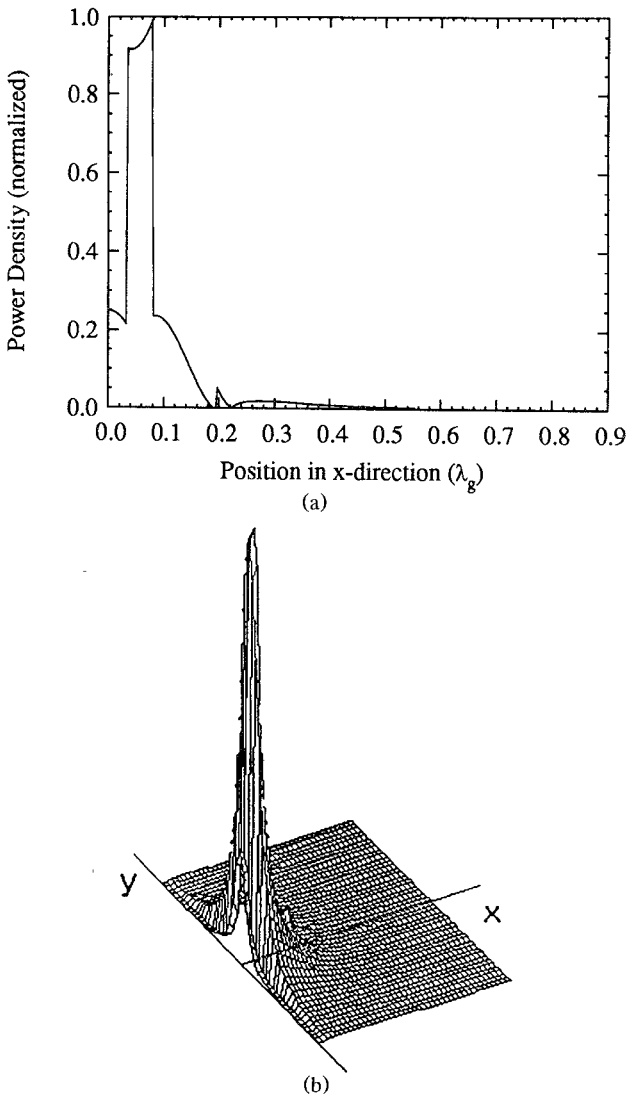

Fig. 8. Power density of the structure designed for 94 GHz. Geometry is described in Fig. 6. (a) Power density along the x-axis at $y = 0$. (b) Power density over the cross-section of the waveguide.

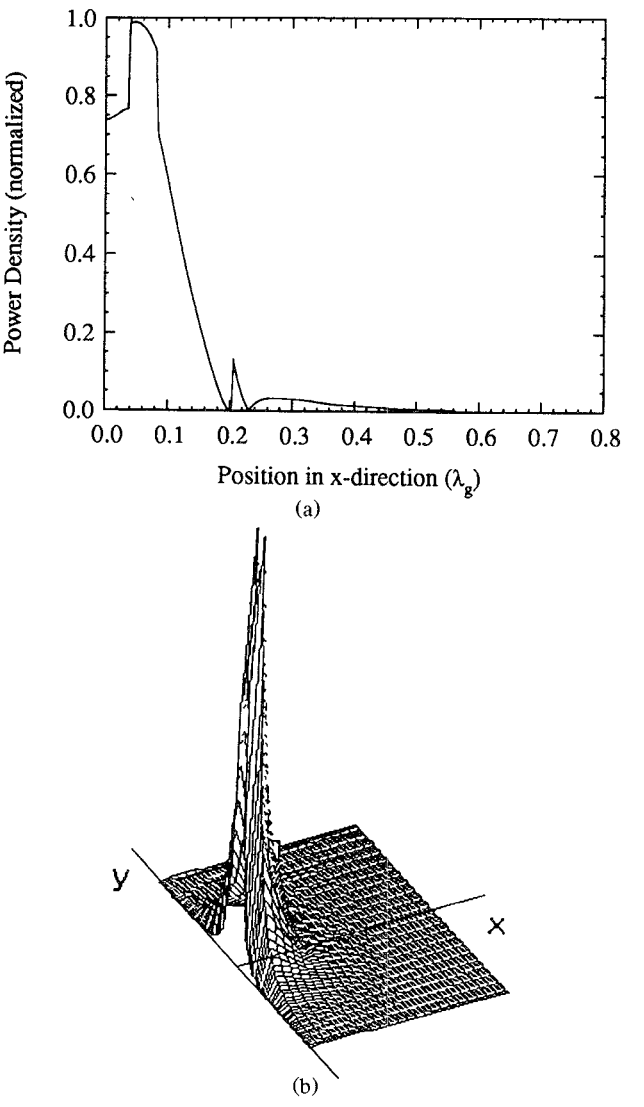

Fig. 9. Power density of the structure designed for 490 GHz. Geometry is described in Fig. 7. (a) Power density along the x-axis at $y = 0$. (b) Power density over the cross-section of the waveguide.

The power density of the dominant mode of each waveguide is extremely well-confined in the respective propagation layers (Figs. 8(a)–(b) and 9(a)–(b)). The power is better concentrated in the propagation layer in the latter example due to the larger contrasts between permittivities in adjacent layers.

After including losses in the dielectric layers, the attenuation constant α of the dominant mode of each structure was calculated as a function of frequency (Figs. 6(b) and 7(b)). For simplicity, the loss tangents were taken to be the worst-case (maximum) values over the frequency ranges, so that the attenuation constants shown in the plots represent upper bounds for the actual values. A worst-case value of 0.002 for the loss tangent of the GaAs layers for frequencies below 400 GHz was obtained from [15]; extrapolation of the data in this reference provided a worst-case value of 0.004 for frequencies up to 1.0 THz. The loss tangent of AlAs was assumed to be comparable to that of GaAs; if the actual losses of AlAs are significantly higher, any material which has a lower loss tangent and is compatible with GaAs may be substituted. Polyamide, when it is prevented from absorbing moisture, is known to exhibit low losses in the sub-mm region, and its loss tangent was taken to be 0.001. Approximate maximum attenuation constant values for the two examples are 0.05 dB/λ_g (18 dB/m) at 94 GHz and 0.19 dB/λ_g (400 dB/m) at 490 GHz, respectively. When the lossless and lossy cases are compared, the phase constants β do not differ significantly.

A simple estimate for the attenuation in the waveguides may be obtained from the formula:

$$\alpha = \frac{\beta}{2} \tan \delta \tag{10}$$

where $\tan \delta$ is the loss tangent of the propagation layer. Equation (10) is derived by assuming that $\tan \delta$ is small and that all propagating power is contained in the propagation layer. Comparisons of the results obtained from the mode-matching technique to the results obtained from

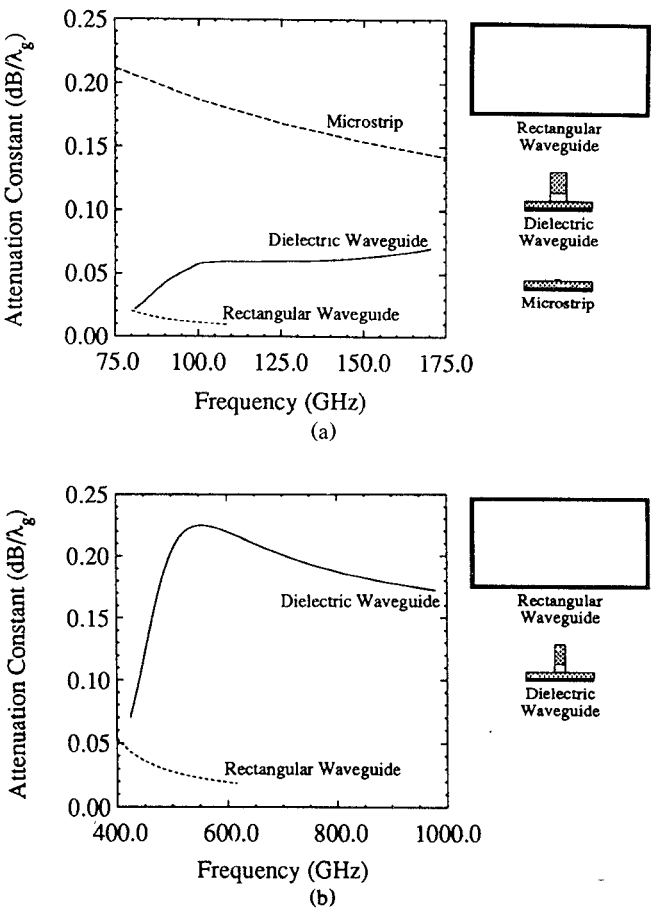

Fig. 10. Comparisons of the attenuation of the structures of Figs. 6 and 7, rectangular waveguide and microstrip. (a) 94 GHz waveguide (Fig. 6) compared to 2.54 mm by 1.27 mm rectangular waveguide with gold sidewalls; and 50 Ω microstrip with $h = 100$ μm, $w = 75$ μm, $\epsilon = 12.85\epsilon_o(1.0 - j0.002)$ (GaAs) and strip conductivity $= 3.33 \times 10^4$ S/mm. Three guiding structures are drawn in the same scale. (b) 490 GHz waveguide (Fig. 7) compared to 0.488 mm by 0.244 mm rectangular waveguide with gold sidewalls (conductivity $= 4.1 \times 10^4$ S/mm). Two guiding structures are drawn in the same scale.

the above formula are included in the attenuation constant plots; these comparisons illustrate the effects of the losses in the non-propagating layers. If the propagation layer can be constructed from a low-loss material (as in the 94 GHz waveguide), and if power confinement in the propagation layer can then be maximized, losses can be minimized. Possibly, increasing the thickness of the propagation layer could improve the power confinement.

The attenuation of the waveguides is contrasted with the attenuation of the conventional rectangular waveguide and microstrip in Fig. 10. The rectangular waveguides were designed with center frequencies comparable to the design frequencies of the monolithic waveguide examples, and the attenuation of the rectangular waveguides from sidewall conductor losses was calculated in accordance with [16]. The microstrip was designed on a substrate comparable to the substrate used for the 94 GHz waveguide, and its attenuation from both conductor and dielectric losses was calculated in accordance with [17]. Due to the impracticality of microstrip at 490 GHz, the microstrip is shown only in comparison to the 94 GHz example. Although the new guiding structures do not have the extremely low attenuation exhibited by the rectangular waveguides, the new waveguides are smaller, and their monolithic nature allows for both easier construction of passive circuit elements (such as couplers, stubs, T-junctions, and inductors) and less arduous integration of active devices and device-waveguide transitions.

V. Conclusion

Low-loss monolithic waveguides have been proposed for sub-mm and THz frequency applications. The design examples have demonstrated a general characteristic of this type of structure; namely, that the materials and structures available in monolithic technology allow the propagating power to be confined in a convenient region at a given frequency. A wide range of designs is available; a different choice of materials, dimensions and layer arrangement could yield waveguides with better power confinement and lower losses than the examples which have been presented.

Future studies will include experimental realization of the waveguides, complete characterization of the waveguides' radiation losses (with the upper conducting plate removed), integration of active devices, design of an active device-to-waveguide transition, and creation of passive circuit elements with the waveguides.

Acknowledgment

The authors would like to thank T. E. van Deventer for the microstrip attenuation data.

References

[1] U. Crombach, "Analysis of single and coupled rectangular dielectric waveguides," *IEEE Trans. Microwave Theory Tech.*, vol. MTT-29, pp. 870-874, Sept. 1981.

[2] R. Mittra, Y. Hou, and V. Jamnejad, "Analysis of open dielectric waveguides using mode-matching techniques and variational methods," *IEEE Trans. Microwave Theory Tech.*, vol. MTT-28, pp. 36-43, Jan. 1980.

[3] K. Solbach and I. Wolff, "The electromagnetic fields and the phase constants of dielectric image lines," *IEEE Trans. Microwave Theory Tech.*, vol. MTT-26, pp. 266-274, Apr. 1978.

[4] W. V. McLevige, R. Mittra, and T. Itoh, "New waveguide structures for millimeter-wave and optical integrated circuits," *IEEE Trans. Microwave Theory Tech.*, vol. MTT-23, pp. 788-794, Oct. 1975.

[5] K. Ogusu, "Numerical analysis of the rectangular dielectric waveguide and its modifications," *IEEE Trans. Microwave Theory Tech.*, vol. MTT-25, pp. 874-885, Nov. 1977.

[6] T. Itoh, "Inverted strip dielectric waveguide for millimeter-wave integrated circuits," *IEEE Trans. Microwave Theory Tech.*, vol. MTT-24, pp. 821-827, Nov. 1980.

[7] T. Itoh and B. Adelseck, "Trapped image guide for millimeter-wave circuits," *IEEE Trans. Microwave Theory Tech.*, vol. MTT-28, pp. 1433-1436, Dec. 1980.

[8] T. Wang and S. E. Schwarz, "Design of dielectric ridge waveguides for millimeter-wave integrated circuits," *IEEE Trans. Microwave Theory Tech.*, vol. MTT-31, pp. 128-134, Feb. 1983.

[9] R. Mittra and S. W. Lee, *Analytical Techniques in the Theory of Guided Waves*. New York: McGraw-Hill, 1961.

[10] S. Peng and A. A. Oliner, "Guidance and leakage properties of a class of open dielectric waveguides: Pt. I-mathematical formulations," *IEEE Trans. Microwave Theory Tech.*, vol. MTT-29, pp. 843-855, Sept. 1981.

[11] A. A. Oliner and S. Peng, "Guidance and leakage properties of a class of open dielectric waveguides: Pt. II—new physical effects," *IEEE Trans. Microwave Theory Tech.*, vol. MTT-29, pp. 855–869, Sept. 1981.
[12] F. E. Gardiol, "Higher-order modes in dielectrically loaded rectangular waveguides," *IEEE Trans. Microwave Theory Tech.*, vol. MTT-16, pp. 919–924, Nov. 1968.
[13] S. Adachi, "GaAs, AlAs, $Al_xGa_{1-x}As$: Material parameters for use in research and device applications," *J. Appl. Phys.*, vol. 58, pp. R1–R29, 1 Aug. 1985.
[14] R. F. Harrington, *Time-Harmonic Electromagnetic Fields*. New York: McGraw-Hill, 1961.
[15] M. N. Afsar and K. J. Button, "Precise millimeter-wave measurements of complex refractive index, complex dielectric permittivity and loss tangent of GaAs, Si, SiO_2, Al_2O_3, BeO, macor, and glass," *IEEE Trans. Microwave Theory Tech.*, vol. MTT-31, pp. 217–223, Feb. 1983.
[16] C. A. Balanis, *Advanced Engineering Electromagnetics*. New York: Wiley, 1989.
[17] T. E. van Deventer, P. B. Katehi, and A. Cangellaris, "An integral equation method for the evaluation of conductor and dielectric losses in high frequency interconnects," *IEEE Trans. Microwave Theory Tech.*, vol. MTT-37, pp. 1964–1972, Dec. 1989.

Andrew Engel, Jr. was born in Rochester, MN on February 9, 1961. He received the B.S. degree in physics from Stanford University, Stanford, CA, in 1982.

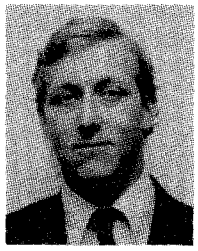

From 1984–1987, he worked at Avantek, Inc., Santa Clara, CA as a Microwave Components Failure Analysis Engineer. Since 1987, he has been enrolled in the graduate program in electrical engineering at The University of Michigan, Ann Arbor, where he received the M.S. degree in 1988. He is currently completing his doctoral dissertation in microwave, millimeter wave and THz hybrid and monolithic waveguiding structures.

Linda P. B. Katehi, (S'81–M'84–SM'89) received the B.S.E.E. degree from the National Technical University of Athens, Greece, in 1977 and the M.S.E.E. and Ph.D. degrees from the University of California, Los Angeles, in 1981 and 1984 respectively.

In September 1984 she joined the faculty of the Electrical Engineering and Computer Science Department of the Universty of Michigan, Ann Arbor. Since then, she has been involved in the modeling and computer-aided design of milimeter-wave and near-millimeter-wave monolithic circuits and antennas.

In 1984 Dr. Katehi received the W. P. King Award and in 1985 the S. A. Schelkunoff Award from the Antennas and Propagation Society. In 1987 she received an NSF Presidential Young Investigator Award and an URSI Young Scientist Fellowship. She is a member of Sigma Xi.